

Brief Report

Biofabricated Aluminium Oxide Nanoparticles Derived from *Citrus aurantium* L.: Antimicrobial, Anti-Proliferation, and Photocatalytic Efficiencies

Punitha Nagarajan ¹, Vijayakumar Subramaniyan ^{1,*}, Vidhya Elavarasan ¹, Nilavukkarasi Mohandoss ¹, Prathipkumar Subramaniyan ² and Sekar Vijayakumar ^{3,*} 

¹ PG and Research Department of Botany, A.V.V.M. Sri Pushpam College, Bharathidasan University, Tiruchirappalli 613503, Tamil Nadu, India

² National Institute of Technology, Tiruchirappalli 620015, Tamil Nadu, India

³ Marine College, Shandong University, Weihai 264209, China

* Correspondence: svijaya_kumar2579@rediff.com (V.S.); vijaysekar05@gmail.com (S.V.)

Abstract: A current strategy in material science and nanotechnology is the creation of green metal oxide nanoparticles. *Citrus aurantium* peel extract was used to create aluminium oxide nanoparticles (Al₂O₃ NPs) in an efficient, affordable, environmentally friendly, and simple manner. Various characterisation methods such as UV-vis spectrophotometer (UV), X-ray diffraction (XRD), Fourier transform infrared spectroscopy (FT-IR), and field emission scanning electron microscopy (FE-SEM) were utilised to assess the morphology of Al₂O₃ NPs. The elemental composition was performed by EDX analysis. Using the well diffusion method, Al₂O₃ NPs' antimicrobial properties were used against pathogenic organisms. The antiproliferation efficacy of a neuronal cell line was investigated using the MTT assay. The photocatalytic activities were studied against methylene blue dye. In this study, Al₂O₃ NPs were found to have an average crystallite size of 28 nm in the XRD, an absorption peak at 322 nm in the UV spectrum, and functional groups from 406 to 432 in the FT-IR spectrum, which were ascribed to the stretching of aluminium oxide. Antimicrobial efficiencies were observed against *Pseudomonas aeruginosa* [36 ± 2.12], *Staphylococcus aureus* [35 ± 1.23], *Staphylococcus epidermis* [27 ± 0.06], *Klebsiella pneumonia* [25 ± 1.65], *Candida albicans* [28 ± 1.06], and *Aspergillus niger* [27 ± 2.23], as well as the cell proliferation of a PC 12 cell line (54.09 at 31.2 µg/mL). Furthermore, photocatalytic degradation of methylene blue dye decreased up to 89.1 percent after 150 min. The current investigation concluded that biosynthesised Al₂O₃ NPs exhibit feasible antimicrobial, anti-proliferative, and photocatalytic behaviours.

Keywords: biofabrication; *Citrus aurantium*; antimicrobial activity; anti-proliferation; photocatalytic activity



Citation: Nagarajan, P.; Subramaniyan, V.; Elavarasan, V.; Mohandoss, N.; Subramaniyan, P.; Vijayakumar, S. Biofabricated Aluminium Oxide Nanoparticles Derived from *Citrus aurantium* L.: Antimicrobial, Anti-Proliferation, and Photocatalytic Efficiencies. *Sustainability* **2023**, *15*, 1743. <https://doi.org/10.3390/su15021743>

Academic Editor: Harvey Hou

Received: 3 December 2022

Revised: 12 January 2023

Accepted: 14 January 2023

Published: 16 January 2023



Copyright: © 2023 by the authors. Licensee MDPI, Basel, Switzerland. This article is an open access article distributed under the terms and conditions of the Creative Commons Attribution (CC BY) license (<https://creativecommons.org/licenses/by/4.0/>).

1. Introduction

Aluminium oxide nanoparticles (Al₂O₃ NPs) are stable crystalline particles over a broad temperature range. They have a structure similar to that of crystals, with oxygen atoms arranged hexagonally near one another and ions of aluminium loading octahedral holes in two-thirds of the lattice [1]. Al₂O₃ nanopowders are made using a variety of traditional chemical and physical processes, such as sol-gel [2], sputtering [3], mechanical milling [4], and hydrothermal [5]. Though there are only a few environmentally friendly processes utilised to create alumina nanoparticles [6].

When compared to their chemically generated equivalents, bioactive components of plant extracts were shown to be harmless to humans, with superior biocompatibility and outstanding antibacterial activities [7]. Due to the possible aldehyde components of its own bioactive chemicals, the natural extract is expected to be beneficial as a chelating agent for bioengineering nanoscale oxides [8]. *Citrus aurantium* L. is a traditional medicinal plant with a wide range of therapeutic applications. It is a rich source of the alkaloid p-synephrine

as well as many other bioactive compounds, including flavonoids. This plant is employed to treat a range of conditions, including anxiety, lung and prostate cancer, obesity, and digestive problems [9]. The lack of physical activity, cerebral worry, and unease today cause people to live disturbing lives. These factors are solidly linked to the progression of several illnesses, including neurodegenerative disorders [10]. Consequently, the current goal of the investigation is to fabricate the Al_2O_3 NPs via *Citrus aurantium* peel extract. In addition, this synthesised nanoparticle has proven amazing antimicrobial, anti-neuronal, and photodegradation activities.

2. Materials and Methods

2.1. Chemicals

Potassium aluminium sulphates ($\text{KAl}(\text{SO}_4)_2 \cdot 12\text{H}_2\text{O}$), zinc acetate ($\text{ZnC}_4\text{H}_6\text{O}_4$), and sodium hydroxide (NaOH) were used in this experiment; all of the chemicals and solvents were provided by Sigma Aldrich Chemicals, India.

2.2. Collection and Preparation of Plant Materials

In May 2019, the peels of the fruit *Citrus aurantium* were purchased at Kamaraj market in Thanjavur, Tamil Nadu, India. The plant was identified and validated by John Brito of the Rapinot Herbarium in Tiruchirappalli, Tamil Nadu, India. Fruit peels were pulverised into a fine powder. Ten grammes of peel powder were extracted with 100 mL of distilled water. After filtering the extract via Whatman No. 1 filter paper, the resultant mixture was taken as a plant extract.

2.3. Synthesis of Aluminium Oxide Nanoparticles

A solution of 0.5 M potassium aluminium sulphate is prepared by using 100 mL of double-distilled water, which is then added to 5 mL of *Citrus aurantium* peel extract. To that, 2 g of sodium hydroxide followed by 2 g of zinc acetate solution were added. A constant pH of 12 was used for the solution after the addition of 4 g of sodium hydroxide, followed by 2 h of continuous stirring. After 2 hours, the solution was centrifuged at 6000 rpm for 30 min. After that, the aqueous solution was heated for 60 min until it transformed into a pale brown adhesive. After that, this adhesive was mixed and heated at 400°C in a muffle furnace. A pale brown powder was the end product, which was carefully gathered and preserved for characterisation.

2.4. Characterisation of Aluminium Oxide Nanoparticles

Utilising UV-vis absorption spectroscopy, the optical properties of biofabricated Al_2O_3 NPs were diluted and investigated at various wavelengths between 250 and 700 nm (Hitachi U-2001). Al_2O_3 NPs' crystallinity was assessed using XRD. The crystalline size and phase purity of the Al_2O_3 NPs were determined using the X-ray diffraction (XRD) technique (Model D8 Advance, BRUKER, Germany). Fourier transform infrared spectroscopy was used to study the functional groups of the nanoparticles (FTIR- Jascov-650 spectrophotometer). Field emission Scanning electron microscopy (FE-SEM, Hi-Tech model s-3400n). The composition of the Al_2O_3 NPs was examined using the Energy Dispersive X-ray (EDX) method.

2.5. Antimicrobial Activity

The antimicrobial activity of aluminium oxide nanoparticles was examined using the agar well diffusion method [11]. This study used Gram-positive bacteria *Staphylococcus aureus* (MTCC737), *Staphylococcus epidermis* (MTCC10656), Gram-negative bacteria *Pseudomonas aeruginosa* (MTCC429), *Klebsiella pneumoniae* (MTCC618), and fungal strains like *Candida albicans* (MTCC227) and *Aspergillus niger* (MTCC281) to investigate the antimicrobial efficiency of the plant extract and biofabricated Al_2O_3 NPs. These were purchased from the Eunice Analytical Lab and Research Institute, Tiruchirappalli, India, and also obtained from the microbial type culture collection (MTCC), Chandigarh. The fungal and

bacterial cultures were subcultured in MHA (Mueller–Hinton Agar) medium at 35 °C and at 30 °C in Sabouraud dextrose agar media, respectively. Gentamycin (5 µg) and nystatin (50 µg) were used as positive controls for bacteria and fungus, respectively.

2.6. Anti-Proliferative Activity

The National Centre for Cell Sciences (NCCS), in Pune, India, provided PC-12 cell cultures. While all research was done on 96 microtiter plates, the stock cultures were made in 25 cm² culture flasks. Trypsinisation of the cell culture and adjustment of the cell density to 1×10^5 cells per well using 10% FBS. Cell viability was determined using MTT assays in accordance with Salameh et al. [12]. The absorbance at 540 nm was measured using a UV spectrophotometer. The 50% (IC₅₀) values for the various sample concentrations used in the cell growth inhibition experiment were determined using the formula below.

$$\% \text{growth inhibition} = \frac{100 - \text{Mean OD of individual group}}{\text{Mean OD of the control group}}$$

2.7. Photocatalytic Activity

Methylene blue (MB) dye was photodegraded via an annular type of photoreaction with aluminium oxide in an aqueous solution, and UV light is produced by a 100 W halogen lamp. In the experiment, 150 mL of MB solution were used to fill the reactant with 50 mg of the substance. The mixture was then sonicated for 30 minutes in the dark to achieve an adsorption behaviour. The reactant-filled methylene blue emulsion is exposed to various durations of visible light irradiation.

2.8. Statistical Analysis

All the tests were done in triplicate. The outcomes were presented as mean ± standard errors, and the antimicrobial activity of the samples was compared to that of conventional antibiotics using one-way analysis of variations.

3. Results and Discussion

3.1. UV-vis Absorption

UV-vis spectroscopy and photoluminescence spectroscopy were used to demonstrate the optical properties of the biofabricated Al₂O₃ NPs at room temperature. By their 322 nm absorption wavelengths, Figure 1 demonstrates the excitonic nature of Al₂O₃ NPs. The current findings were in strong comparison to previous reports of an absorption peak for the biogenesis of Al₂O₃ NPs at 326 nm [11].

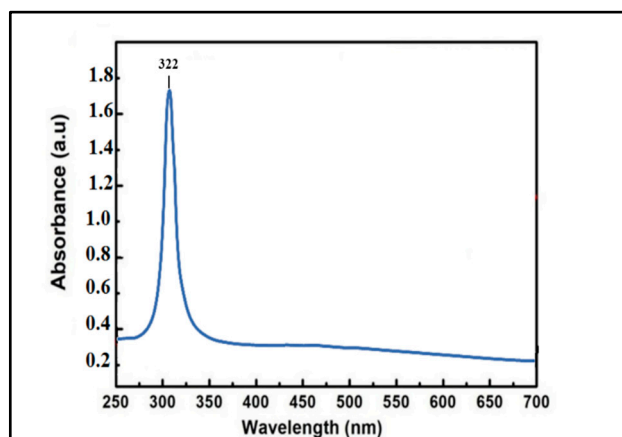


Figure 1. UV-vis absorption of Al₂O₃ NPs.

3.2. X-ray Diffraction Pattern

The X-ray diffraction image of the biofabricated Al_2O_3 NPs is shown in Figure 2. The indexes for the diffraction peaks at the corresponding planes $2\theta = 27.2, 34.8, 44.7, 55.4, 59.9,$ and 66.3 are (220), (311), (400), (422), (511), and (440). The sample's peak intensity indicates a higher rate of crystalline structure and a predictable structure, as seen in the illustration. As the peak's breadth increased, the particle size decreased. This finding is in accordance with the literature, which has been published by Duraisamy [13]. The crystallite size of the nanoparticles was 28 nm, which is the common nanoparticle size. The Debye–Scherrers formula can be used to predict the crystal size of the derived NPs [10].

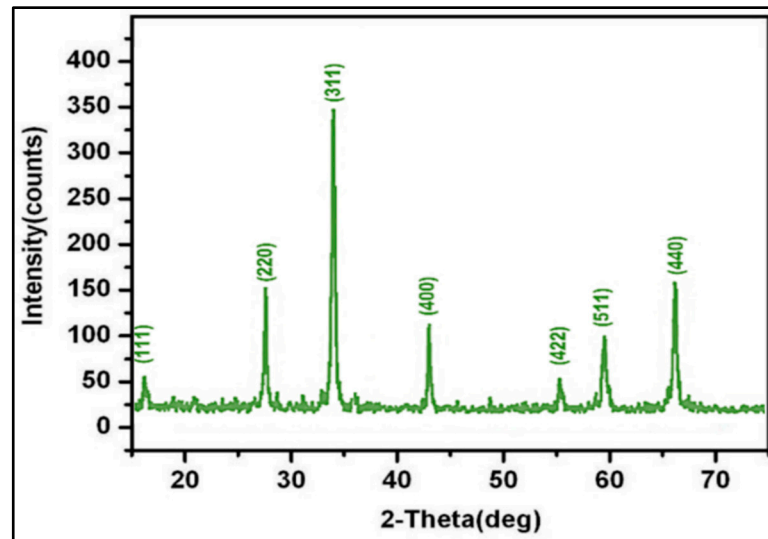


Figure 2. XRD patterns of Al_2O_3 NPs.

3.3. FT-IR Analysis

The FT-IR investigation of biofabricated Al_2O_3 NPs from fruit peel extract exposes numerous functional groups, which were observed in the range of $406\text{--}3412\text{ cm}^{-1}$ (Figure 3). The peaks at 406 cm^{-1} , 1110 cm^{-1} , and 1369 cm^{-1} are conspicuous peaks of Al_2O_3 NPs [11]. The peaks at 432 cm^{-1} , 584 cm^{-1} , and 830 cm^{-1} are because of Al-O-Al bonds [13]. An absorption peak at 1620 cm^{-1} and 3412 cm^{-1} is owing to the presence of C-O-C stretching [14].

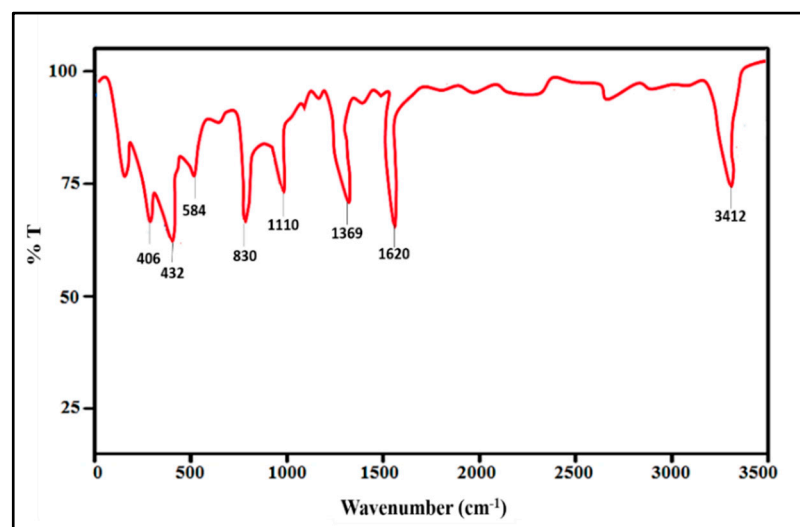


Figure 3. FT-IR spectrum of Al_2O_3 NPs.

3.4. FE-SEM with EDAX Analysis

The usage of FE-SEM analysis was to analyse the structure of biofabricated Al_2O_3 NPs, and the results are displayed in Figure 4a with an agglomerated micrograph. It is evident that the structure of biofabricated Al_2O_3 NPs is spherical. To ascertain the elemental makeup and purity of Al_2O_3 NPs, EDAX analysis was performed. The sharp, lengthy peaks indicate the purity and atomic composition of the elements Al and O (Figure 4b). The histogram of the 28 nm particle size distribution of biofabricated Al_2O_3 NPs is shown in Figure 4c.

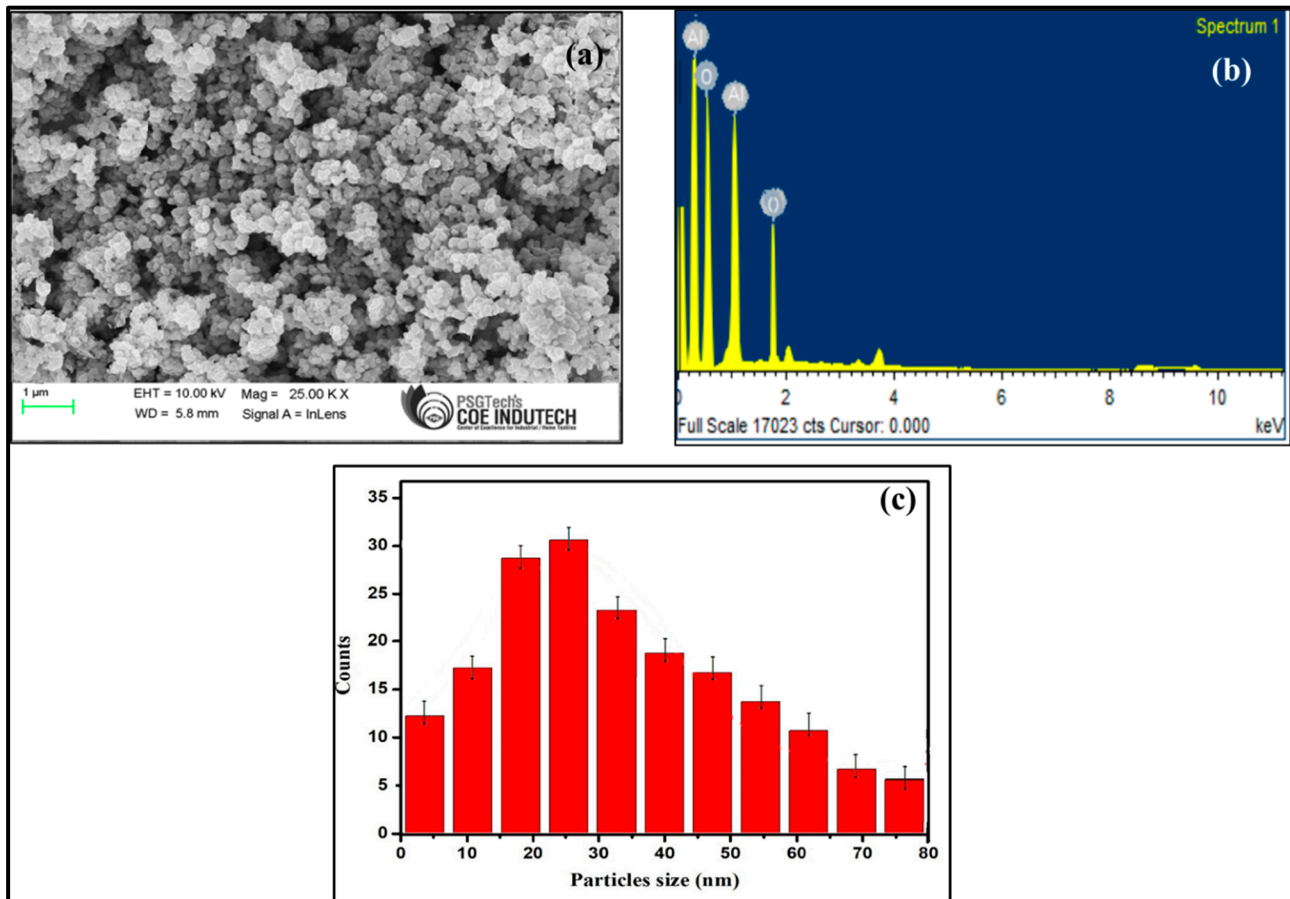


Figure 4. (a) FE-SEM image of Al_2O_3 NPs, (b) EDAX analysis of Al_2O_3 NPs, and (c) histogram distribution of Al_2O_3 NPs.

3.5. Antimicrobial Activity

Al_2O_3 NPs' antimicrobial properties were studied against pathogens like *Staphylococcus aureus*, *Staphylococcus epidermis*, *Pseudomonas aeruginosa*, *Klebsiella pneumoniae*, *Candida albicans*, and *Aspergillus niger* (Figure 5). Results showed that the Al_2O_3 NPs produced had strong antimicrobial action, with potent efficacy values for *P. aeruginosa* (36 ± 2.12), *S. aureus* (35 ± 1.23), *S. epidermis* (27 ± 0.06), *K. pneumoniae* (25 ± 1.65), *C. albicans* (28 ± 1.06), and *A. niger* (27 ± 2.23). Furthermore, a larger zone of inhibition was observed in *S. aureus* and *P. aeruginosa* when compared to control biofabricated Al_2O_3 NPs (Figure 6). A similar approach was noticed by Manogar et al. [11], who reported that Al_2O_3 NPs' inhibitory impact increased when concentration was increased, but their activities other than *Klebsiella pneumoniae* and *Candida albicans* had a similar inhibiting effect (22 mm). The least inhibition activity was observed in *Klebsiella pneumoniae* using *Citrus aurantium* peel extract. Manyashree et al. [1] reported similar findings.

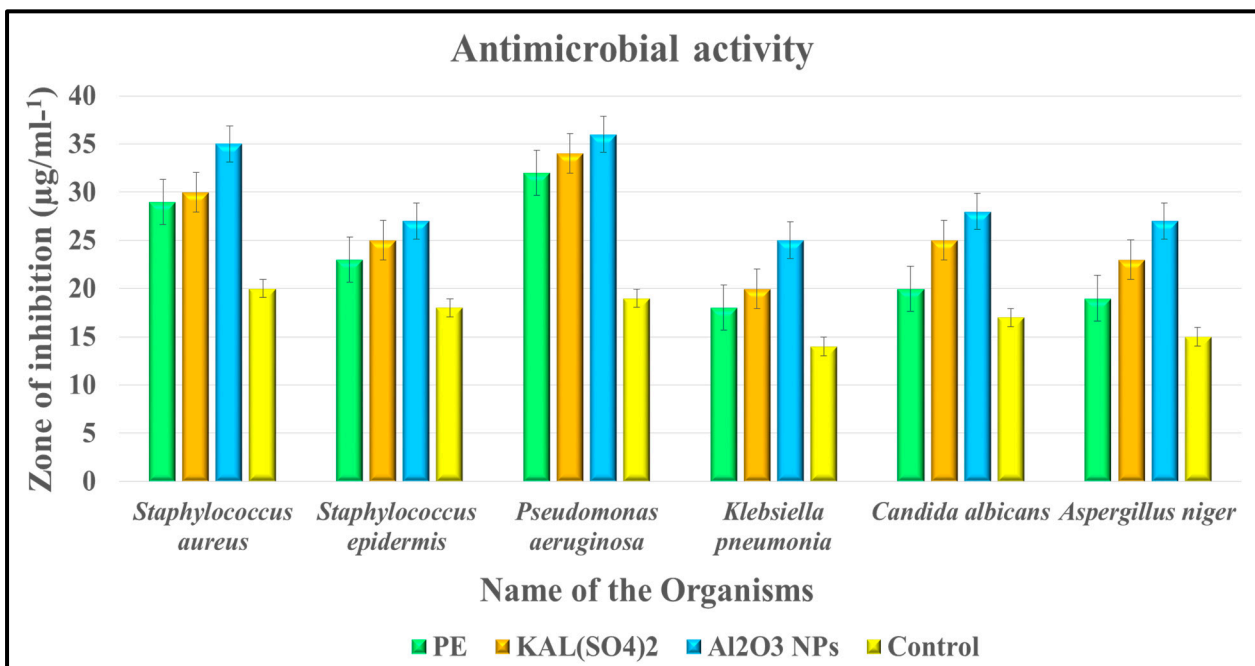


Figure 5. Antimicrobial analysis of biofabricated Al₂O₃ NPs against pathogens.

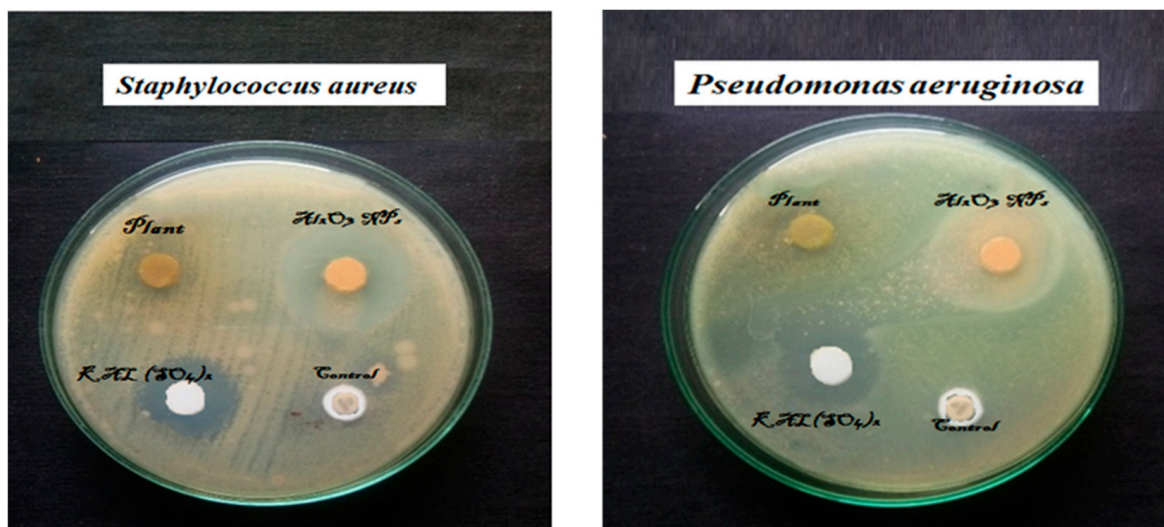


Figure 6. Antimicrobial evaluation of biofabricated Al₂O₃ NPs using the well method.

3.6. Antiproliferative Activity

The results of cytotoxicity investigations using the PC12 cell line and MTT analysis of biofabricated Al₂O₃ NPs were reported in this work, and the results were 54.09% at 31.2 µg/mL. (Figure 7a). It indicates that the IC₅₀ values for the biofabricated Al₂O₃ NPs are 31.2 and 62.5 µg/mL. During 24 h of treatment with various concentrations of biofabricated Al₂O₃ NPs, the PC12 cell line's morphological analysis is displayed in Figure 7b.

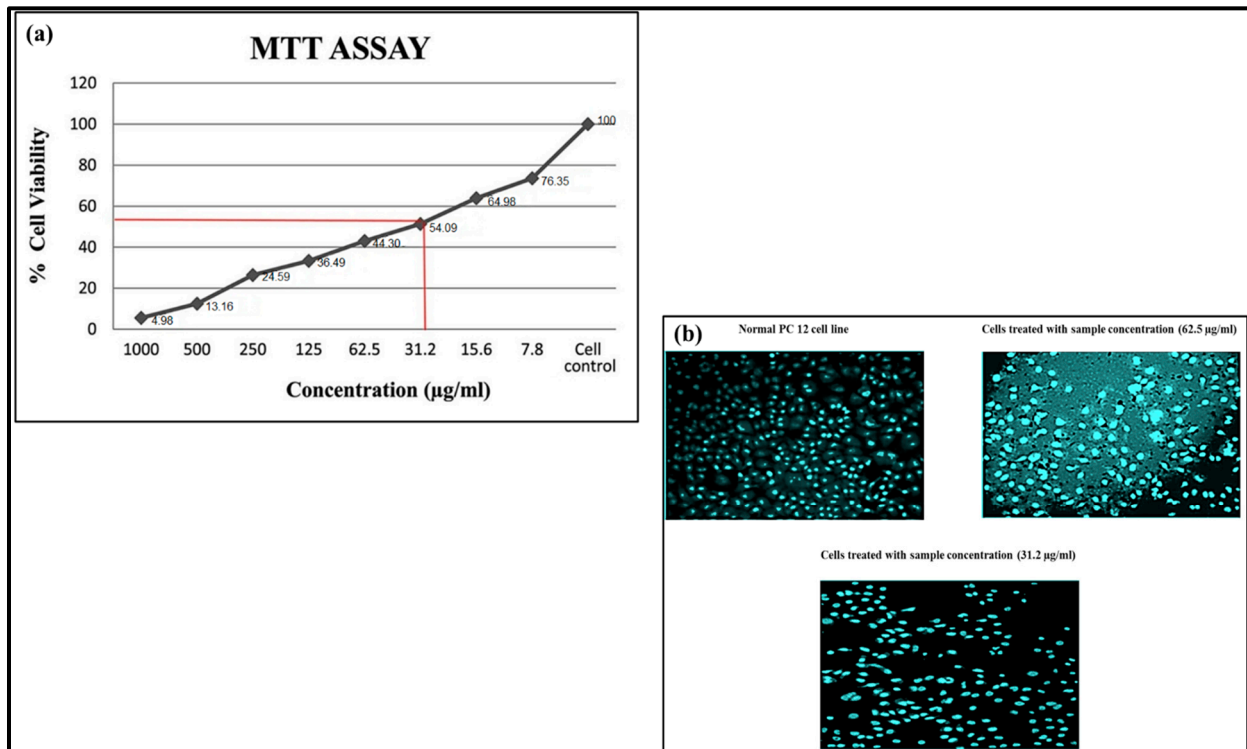


Figure 7. (a) Cytotoxic effect of Al_2O_3 NPs using MTT assay and (b) anti-proliferative effects of a human neuronal cell line (PC 12).

3.7. Photocatalytic Activity

The photodegradation capability of biofabricated Al_2O_3 NPs and the absorption spectra for MB dye degradation are shown in Figure 8. Visible light does not exhibit an absorption spectrum peak, and the typical absorption maximum peak of MB dye appears at 665 nm. The band of MB's absorption is reduced with respect to time by the addition of biofabricated Al_2O_3 NPs. Within 150 min, the MB dye's absorption band fully deteriorated, with a maximum percentage of 89.1%. Accordingly, Kiran Kumar et al. [15] found that using 10 mg of $\gamma\text{-Al}_2\text{O}_3$ as a photocatalyst under sunlight resulted in 91.6% MB photodegradation in 240 min. Metal oxide nanoparticles such as ZnO, NiO, palladium oxide, and CuO have also been investigated for their electrochemical activity and have proven to be viable electrocatalysts. [16–18].

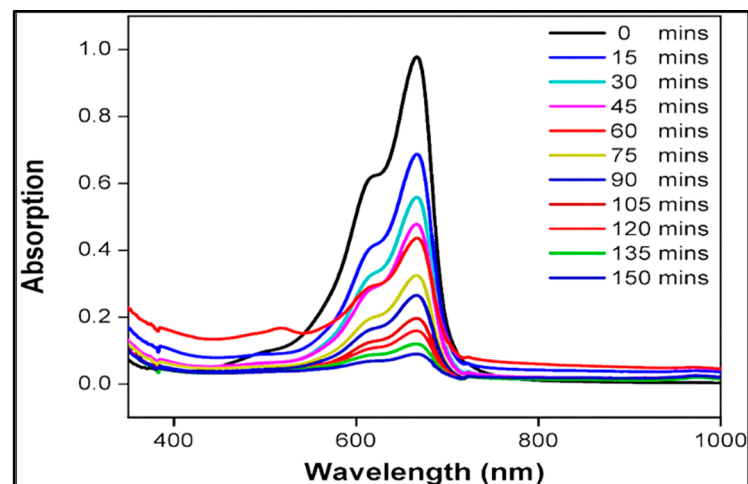


Figure 8. Photodegradation of MB with biofabricated Al_2O_3 NPs.

4. Conclusions

Based on the findings, it was determined that biofabricated Al₂O₃ NPs were successfully synthesised by *Citrus aurantium* fruit peel extract. The parameters of the generated Al₂O₃ NPs, including their structural, optical, elemental, and morphological characteristics, were examined using UV-vis spectroscopy, XRD, FE-SEM with EDX, and FTIR. The purity and composition of the biofabricated Al₂O₃ NPs can be observed by the sharp, lengthy peaks in the EDAX analysis. The study established amazing antimicrobial activity, specifically in *S. aureus* and *P. aeruginosa*, and anti-neuronal activity results show 54.09% at 31.2 µg/mL. Additionally, photodegradation efficiency is admirable with 89.1% dye degradation.

Author Contributions: Synthesised nanoparticles and investigated the antiproliferative activity, P.N.; conceptualisation and monitored the overall setup, manuscript—writing, S.V.; data analysis of characterisations of nanoparticles, V.S., V.E., N.M., P.S. and S.V. All authors have read and agreed to the published version of the manuscript. All authors have helped to finish the paper.

Funding: The authors are appreciative of the financial support provided by the DST-FIST (SR/FST/College-222/2014) and DBT-STAR (HRD-11011/18/2022-HRD-DBT) for this study.

Institutional Review Board Statement: Not Applicable.

Informed Consent Statement: Not Applicable.

Data Availability Statement: On behalf of all the authors, the corresponding author states that our data are available upon reasonable request.

Acknowledgments: The authors are appreciative of the financial support provided by the DST-FIST (SR/FST/College-222/2014) and DBT-STAR (HRD-11011/18/2022-HRD-DBT) for this study. We gratefully thank the administration of A.V.V.M. Sri Pushpam College (Autonomous), Poondi, for providing us with the resources and assistance we needed to complete this task.

Conflicts of Interest: The authors have declared no conflict of interest.

References

1. Manyasree, D.; Kiranmayi, P.; Ravi Kumar, R.V.S.S.N. Synthesis, characterization and antibacterial activity of aluminium oxide nanoparticles. *Int. J. Pharm. Pharm. Sci.* **2018**, *10*, 32–35. [[CrossRef](#)]
2. Yang, H.; Ouyang, J.; Tang, A.; Xiao, Y.; Li, X.; Dong, X.; Yu, Y. Electrochemical synthesis and photocatalytic property of cuprous oxide nanoparticles. *Mater. Res. Bull.* **2006**, *41*, 1310–1318. [[CrossRef](#)]
3. Trinh, D.H.; Ottosson, M.; Beckers, M.; Collin, M.; Reineck, I.; Hultman, L.; Högberg, H. Structural and mechanical characterisation of nanocomposite Al₂O₃-ZrO₂ thin films grown by reactive dual radiofrequency magnetron sputtering. *Thin Solid Film.* **2008**, *516*, 4977–4982. [[CrossRef](#)]
4. Reid, C.B.; Forrester, J.S.; Goodshaw, H.J.; Kisi, E.H.; Suaning, G.J. A study in the mechanical milling of alumina powder. *Ceram. Int.* **2008**, *34*, 1551–1556. [[CrossRef](#)]
5. Qu, L.; He, C.; Yang, Y.; He, Y.; Liu, Z. Hydrothermal synthesis of alumina nanotubes templated by anionic surfactant. *Mater. Lett.* **2005**, *59*, 4034–4037. [[CrossRef](#)]
6. Hasanpoor, M.; Nabavi, H.F.; Aliofkhaezrai, M. Microwave-Assisted Synthesis of Alumina Nanoparticles Using Some Plants Extracts. *J. Nanostruct.* **2017**, *7*, 40–46. [[CrossRef](#)]
7. Khalil, A.T.; Ovais, M.; Ullah, I.; Ali, M.; Shinwari, Z.K.; Maaza, M. Biosynthesis of iron oxide (Fe₂O₃) nanoparticles via aqueous extracts of *Sageretia thea* (Osbeck.) and their pharmacognostic properties. *Green Chem. Lett. Rev.* **2017**, *10*, 186–201. [[CrossRef](#)]
8. Ditlopo, N.; Sintwa, N.; Khamlich, S.; Manikandan, E.; Gnanasekaran, K.; Henini, M.; Gibaud, A.; Krief, A.; Maaza, M. From Khoi-San indigenous knowledge to bioengineered CeO₂ nanocrystals to exceptional UV-blocking green nanocosmetics. *Sci. Rep.* **2022**, *12*, 3468. [[CrossRef](#)] [[PubMed](#)]
9. Vijayakumar, S.; Punitha, V.N.; Parameswari, N. Phytonanosynthesis of MgO Nanoparticles: Green Synthesis, Characterization and Antimicrobial Evaluation. *Arab. J. Sci. Eng.* **2021**, *47*, 6729–6734. [[CrossRef](#)]
10. Punitha, V.N.; Vijayakumar, S.; Sakthivel, B.; Praseetha, P.K. Protection of neuronal cell lines, antimicrobial and photocatalytic behaviours of eco-friendly TiO₂ nanoparticles. *J. Environ. Chem. Eng.* **2020**, *8*, 104343. [[CrossRef](#)]
11. Manogar, P.; Morvinyabesh, J.E.; Ramesh, P.; Jeyaleela, G.D.; Amalan, V.; Ajarem, J.S.; Allam, A.A.; Khim, J.S.; Vijayakumar, N. Biosynthesis and antimicrobial activity of aluminium oxide nanoparticles using *Lyngbya majuscula* extract. *Mater. Lett.* **2022**, *311*, 131569. [[CrossRef](#)]
12. Salameh, B.A.; Cumpstey, I.; Sundin, A.; Leffler, H.; Nilsson, U.J. 1H-1,2,3-Triazol-1-yl thiodigalactoside derivatives as high affinity galectin-3 inhibitors. *Bioorg. Med. Chem.* **2018**, *18*, 5367–5378. [[CrossRef](#)] [[PubMed](#)]

13. Duraisamy, P. Green Synthesis of Aluminium Oxide Nanoparticles by using Aerva Lanta and Terminalia Chebula Extracts. *IJRASET* **2018**, *6*, 428–433. [[CrossRef](#)]
14. Sutradhar, P.; Debnath, N.; Saha, M. Microwave-assisted rapid synthesis of alumina nanoparticles using tea, coffee and triphala extracts. *Adv. Manuf.* **2013**, *1*, 357–361. [[CrossRef](#)]
15. Anna, K.K.; Bogireddy, N.K.R.; Agarwal, V.; Bon, R.R. Synthesis of α and γ phase of aluminium oxide nanoparticles for the photocatalytic degradation of methylene blue under sunlight: A comparative study. *Mater. Lett.* **2022**, *317*, 132085. [[CrossRef](#)]
16. Matinise, N.; Fuku, X.; Kaviyarasu, K.; Mayedwa, N.; Maaza, M. ZnO nanoparticles via Moringa oleifera green synthesis: Physical properties & mechanism of formation. *Appl. Surf. Sci.* **2017**, *406*, 339–347. [[CrossRef](#)]
17. Mayedwa, N.; Mongwaketsi, N.; Khamlich, S.; Kaviyarasu, K.; Matinise, N.; Maaza, M. Green synthesis of nickel oxide, palladium and palladium oxide synthesized via Aspalathus linearis natural extracts: Physical properties & mechanism of formation. *Appl. Surf. Sci.* **2010**, *446*, 266–272. [[CrossRef](#)]
18. Rathnakumar, S.S.; Noluthando, K.; Kulandaiswamy, A.J.; Rayappan, J.B.B.; Kasinathan, K.; Kennedy, J.; Maaza, M. Stalling behaviour of chloride ions: A non-enzymatic electrochemical detection of α -Endosulfan using CuO interface. *Sens. Actuators B Chem.* **2019**, *293*, 100–106. [[CrossRef](#)]

Disclaimer/Publisher’s Note: The statements, opinions and data contained in all publications are solely those of the individual author(s) and contributor(s) and not of MDPI and/or the editor(s). MDPI and/or the editor(s) disclaim responsibility for any injury to people or property resulting from any ideas, methods, instructions or products referred to in the content.